

Article

# Effect of Hydrogen Bond Donors and Acceptors on CO<sub>2</sub> Absorption by Deep Eutectic Solvents

Tausif Altamash <sup>1</sup>, Abdulkarem Amhamed <sup>1</sup>, Santiago Aparicio <sup>2,\*</sup> and Mert Atilhan <sup>3,\*</sup>

<sup>1</sup> Qatar Environment & Energy Research Institute, Hamad Bin Khalifa University, Doha 34110, Qatar; taltamash@hbku.edu.qa (T.A.); aamhamed@hbku.edu.qa (A.A.)

<sup>2</sup> Department of Chemistry, University of Burgos, 09001 Burgos, Spain

<sup>3</sup> Department of Chemical and Paper engineering, Western Michigan University, Kalamazoo, MI 49008, USA

\* Correspondence: sapar@ubu.es (S.A.); mert.atilhan@wmich.edu (M.A.)

Received: 7 November 2020; Accepted: 22 November 2020; Published: 25 November 2020



**Abstract:** The effects of a hydrogen bond acceptor and hydrogen bond donor on carbon dioxide absorption via natural deep eutectic solvents were studied in this work. Naturally occurring non-toxic deep eutectic solvent constituents were considered; choline chloride, b-alanine, and betaine were selected as hydrogen bond acceptors; lactic acid, malic acid, and fructose were selected as hydrogen bond donors. Experimental gas absorption data were collected via experimental methods that uses gravimetric principles. Carbon dioxide capture data for an isolated hydrogen bond donor and hydrogen bond acceptor, as well as natural deep eutectic solvents, were collected. In addition to experimental data, a theoretical study using Density Functional Theory was carried out to analyze the properties of these fluids from the nanoscopic viewpoint and their relationship with the macroscopic behavior of the system, and its ability for carbon dioxide absorption. The combined experimental and theoretical reported approach work leads to valuable discussions on what is the effect of each hydrogen bond donor or acceptor, as well as how they influence the strength and stability of the carbon dioxide absorption in deep eutectic solvents. Theoretical calculations explained the experimental findings, and combined results showed the superiority of the hydrogen bond acceptor role in the gas absorption process, with deep eutectic solvents. Specifically, the cases in which choline chloride was used as hydrogen bond acceptor showed the highest absorption performance. Furthermore, it was observed that when malic acid was used as a hydrogen bond donor, it led to low carbon dioxide solubility performance in comparison to other studied deep eutectic solvents. The cases in which lactic acid was used as a hydrogen bond donor showed great absorption performance. In light of this work, more targeted, specific, deep eutectic solvents can be designed for effective and alternative carbon dioxide capture and management.

**Keywords:** absorption; carbon dioxide capture; deep eutectic solvents; density functional theory; hydrogen bond

## 1. Introduction

In recent years, the unprecedented amount of carbon dioxide (CO<sub>2</sub>) emissions, resulting mainly from fossil fuel utilization/based activities, have impacted global warming [1,2] and climate change [3–5]. Conventional amine-based CO<sub>2</sub> mitigation techniques have been considered as effective CO<sub>2</sub> capture methods over the past several decades, despite some serious drawbacks, such as solvent loss, corrosion, degradation and, more importantly, high regeneration energy cost [6–12]. Hence, there is need for alternative solvent systems that can effectively scrub CO<sub>2</sub> in gaseous effluent streams, at both pre- and post- combustion processes, with minimum requirement of infrastructure retrofitting costs for existing CO<sub>2</sub> capture process units in plants. For this purpose, various materials have been developed

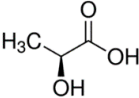
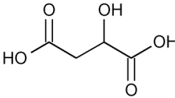
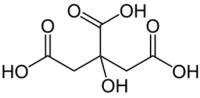
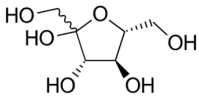
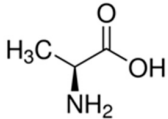
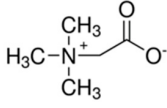
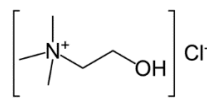
over the past few decades. Porous adsorbents [13–17] as well as liquid solvents [18,19] have been considered in both academia and in the industry; however, due to low manufacturing costs and less requirements on new processing equipment, liquid systems have been considered more attractive. Novel solvent development for CO<sub>2</sub> capture purposes has been centered on ionic liquids [20–25] and liquid polymers [26–29]. In recent years, deep eutectic solvents (DES) [30–32] obtained from ionic liquids, as well as from natural products (natural deep eutectic solvents (NADES)) [33–35], have also been considered for CO<sub>2</sub> management, especially at low to moderate pressures. DES have important advantages over the other potential candidates as they are low-cost materials with appreciable renewability capability [36,37], low toxicity [32,38,39], have less environmental impact [40,41], and good solvent recovery ratio [42].

DES or NADES are formed by mixing the combination of hydrogen bond donors (HBD) and hydrogen bond acceptors (HBA) at various molar mixing ratios to form a low melting point eutectic mixture. Experimental studies show that DES and NADES samples yield to CO<sub>2</sub> solubility that can be compared to current state-of-the-art methods [43]. Several studies on gas solubility in DES with ionic liquids are being used as HBA [30,44–47]. In contrast with DES, only a handful of studies use NADES for CO<sub>2</sub> solubilities; these studies focus mainly on choline chloride as HBA mixed with glycerol/propanediol/malic acids [34] and monoethanolamine [48]. In our previous work, we studied gas absorption performances via novel NADES, which was obtained by considering choline chloride (ChCl), alanine (Al), and betaine (Be) as HBA, and lactic acid (La), malic acid (Ma), and phenylacetic acid (Paa) as HBD. We showed that these NADES perform very well for CO<sub>2</sub> capture, especially at moderate pressures up to 50 bars, and between 298.15 K and 323.15 K isotherms [49–51]. CO<sub>2</sub> sorption experiments showed maximum absorption performance between 3.5 and 5 mmol CO<sub>2</sub>/gr of NADES in these experiments at the highest pressures. Considering the monoethanolamine solution (MEA) CO<sub>2</sub> capture performance as 1.8 mmol CO<sub>2</sub>/g MEA (117 mg/g) at 24 bar and 313 K [52], CO<sub>2</sub> absorption via NADES have great potential for chemical processes. Despite these promising results, there is no systematic study on how HBA/HBD affect the gas sorption performance, what binding role HBA/HBD play during CO<sub>2</sub> capture, which HBA/HBD have a superior effect once exposed to CO<sub>2</sub> environment, and whether ionic liquid based HBA perform better than the amino acidic-based ones. In this work, we attempt to find answers to these questions, present new CO<sub>2</sub> capture data for HBA and HBD, and compare their performances against their NADES mixtures. Furthermore, detailed density functional theory (DFT) calculations were carried out to explain the details of the binding energies and infer on the CO<sub>2</sub> interaction mechanism of HBA/HBD/NADES separately.

## 2. Materials and Methods

The following were purchased from Sigma Aldrich: alanine (Al) with ≥98% purity (Chemical Abstracts Service (CAS) number 56-41-7) with melting point of 258 °C; betaine (Be) with ≥98% purity (CAS number 107-43-7) with melting point of 310 °C; choline chloride (ChCl) with ≥98.0% purity (CAS number 67-48-1) with melting point of 302 °C; DL-malic acid (Ma) with 99.0% purity (CAS number 6915-15-7); lactic acid (La) with 85% purity (CAS number 50-21-5); d-fructose (Fr) with ≥99% purity (CAS number 57-48-7); and citric acid (Ca) with ≥99.5% purity (CAS number 77-92-9). All materials with mentioned purities on the boxes were used without further treatment. Carbon dioxide (CO<sub>2</sub>) gas with purity of ≥99.99% was obtained from Praxair. In order to form NADES samples, Al, Be, ChCl, were mixed with La, Ma, Ca, and Fr with 1 to 1 (1:1) molar mixing ratios by following vigorous stirring of the mixture until a clear-homogenous solution was obtained, in a glove box, in which humidity and ambient conditions were controlled. Table 1 shows the chemical structures of the studied HBA and HBD, which also form the NADES samples, Al:La, Al:Ma, Be:La, ChCl:Ma, ChCl:La, ChCl:Fr. All of the prepared NADES samples were observed to be liquid state at room temperature and at atmospheric pressure. Structures of the HBA and HBD are provided in Table 1.

**Table 1.** Structures of hydrogen bond acceptors (HBA) and hydrogen bond donors (HBD) compounds.

Hydrogen Bond Donor (HBD)				
	Lactic Acid	Malic Acid	Malic Acid	Fructose
Hydrogen Bond Acceptor (HBA)				
	Alanine	Betaine	Choline Chloride	

### 2.1. Experimental

CO<sub>2</sub> sorption performance of NADES samples were reported in a previous study, in which the contactless magnetic suspension gravimetric method was used for high-pressure gas absorption-desorption measurements via Rubotherm apparatus. A magnetic suspension apparatus that is equipped with an automated syringe pump was used to conduct both low- and high-pressure gas experiments. In a typical procedure, a few ml of sample is placed in a measurement chamber and it is evacuated overnight at temperatures around 70 °C. Once the material preparation is complete, then solubility measurements take place in the apparatus, starting from the lower pressures toward higher pressures, with stepwise gradual pressure increments. It takes about 60 min to establish equilibrium thermal in between each pressure increment. Once the highest pressure is measured, then few pressure points are re-experimented during the desorption period, in order to observe whether hysteresis occurs during the reversed conditions. The described method was used to obtain HBA + CO<sub>2</sub> and HBD + CO<sub>2</sub> sorption performances in this work, and further details of the measurement technique, calibration, and overall uncertainty can be obtained elsewhere [53].

### 2.2. Theoretical

Initial structures for all of the considered HBA, HBD compounds, and NADES molecular clusters were built with the Avogadro program [54]; ORCA code [55] was used for DFT calculations along this study for B3LYP functional [56,57], coupled with van der Waals semi-empirical contribution from the DFT-D3 method by Grimme [58], and 6-311++G\*\* basis set. The interaction energy ( $\Delta E$ ) for all of the considered structures were calculated by considering counterpoise correction for Basis Set Superposition Error (BSSE) [59]. The quantum Bader's atoms-in-molecules (AIM) theory [60] was used for interpretation of intermolecular interactions, and for topological analysis, which was obtained via Multiwfn program [61]. From this analysis, specifically interaction regions that were characterized by bond critical points (BCP, (3,-1) type, according to Bader's terminology). The corresponding values of electron density,  $\rho$ , and Laplacian ( $\nabla$ ) of electron density,  $\nabla^2\rho$  were obtained [62]. The properties of the inferred critical points may be related with the strength of the interactions [63,64]. Likewise, quantitative bond critical points and its implications on bonding strength were further analyzed via reduced density gradient analysis (RDG) for visual representation of strength and the nature of intermolecular forces through colored isosurfaces [65].

## 3. Results

CO<sub>2</sub> solubility experiments for NADES molecular structures were reproduced from previous work. In this study, experimental data on CO<sub>2</sub> capture performance via HBA and HBD were received successfully and illustrated graphically. For comparison purposes, 298.15 K isotherm was considered for qualitative and quantitative analysis. A total of 24 pressure points were collected for each HBA or HBD during CO<sub>2</sub> sorption experiments, in which 12 were for adsorption, and 12 for desorption measurements. Figure 1 shows the CO<sub>2</sub> capture performance for HBA and HBD prior to mixing to

form the deep eutectic solvent at 298.15 K isotherm. At a low-pressure side ( $p < 5$  bars), there is no distinct effect observed on the sorption performance and the data are clustered around  $\sim 0.3$  mmol CO<sub>2</sub>/g sorbent. As the pressure is increased to moderate to high pressures, there is a clear separation between ChCl + CO<sub>2</sub>, Be + CO<sub>2</sub> ( $\sim 4.95$  mmol CO<sub>2</sub>/g) cases in comparison to Al + CO<sub>2</sub>, La + CO<sub>2</sub>, Ma + CO<sub>2</sub>, Ca + CO<sub>2</sub> ( $\sim 3.77$  mmol CO<sub>2</sub>/g) cases. However, Fr + CO<sub>2</sub> falls in between of the trend of these two groups at high pressures yielding 4.45 mmol CO<sub>2</sub>/g performance.

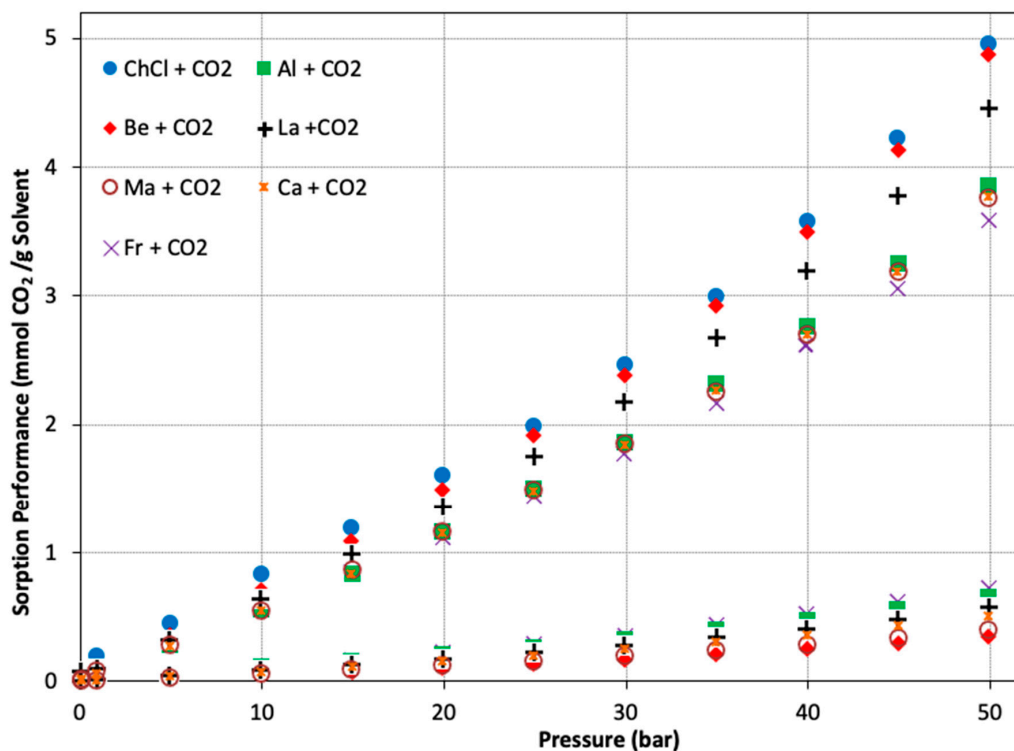


**Figure 1.** CO<sub>2</sub> capture performance for hydrogen bond acceptors and hydrogen bond donors prior to mixing to form deep eutectic solvent at 298.15 K isotherm.

Furthermore, absorption capacity of DES is provided in electronic supporting information for CO<sub>2</sub> loading amounts in mol/mol units. Figure S1 reveals significant trends on the effect of hydroxyl groups. As the amount of hydroxyl groups in the HBD increases, the absorption capacity of the CO<sub>2</sub> increase. This is related to the intramolecular and intermolecular hydrogen-bonding forces between the HBA and the CO<sub>2</sub> molecule. For La, Ma, Fr, Ca there are 4, 3, 2, 1 hydroxyl groups in the HBD structure, and the absorption capacity in Figure S1 overlaps with this argument. On the other hand, for the case of HBA, as the volume of the group that is attached on the N atom in the HBA structure increases, it affects the distance between center of mass and the CO<sub>2</sub> molecule and, thus, develops a hydrogen bond easier. This leads to the hydrogen-bonding force of DES and improved solvent properties. This phenomenon is also observed in this work when the molecular structures of ChCl, Be, and Al are considered, and their CO<sub>2</sub> sorption capacities are examined in Figure S1. The development of hydrogen bonding is discussed in further detail, from the molecular point of view, in the following section of this manuscript.

CO<sub>2</sub> capture performance comparison of the HBA and HBD with respect to NADES has been studied and presented in Figure 2. It was expected for NADES (or DES) CO<sub>2</sub> capture performance to fall in between its former HBA and HBD compounds. However, interestingly, only Al:La + CO<sub>2</sub> showed this behavior with distinct performance separation between the HBA and HBD CO<sub>2</sub> capture data, and fall right in the middle of these two curves (Figure 2a). For the case of ChCl:La + CO<sub>2</sub>, the NADES sorption coincide over the ChCl + CO<sub>2</sub> curve, which is observed to be underperforming

in comparison to La + CO<sub>2</sub> case (Figure 2c). For Al:MA + CO<sub>2</sub> case, it has a similar trend with ChCl:La + CO<sub>2</sub> and the NADES + CO<sub>2</sub> trend overlaps again with the HBA trend (Figure 2d), with the exception of a slight departure of NADES towards higher performance at pressures higher than 35 bars. However, for the case of Al:La + CO<sub>2</sub>, there is a distinct segregation of HBA+CO<sub>2</sub>, HBD+CO<sub>2</sub> and NADES+CO<sub>2</sub> trends (Figure 2c). In this specific case, pressures above 10 bars, CO<sub>2</sub> capture performance trend was observed as La + CO<sub>2</sub> > NADES + CO<sub>2</sub> > Al + CO<sub>2</sub>, or in other words HBD + CO<sub>2</sub> > NADES + CO<sub>2</sub> > HBA + CO<sub>2</sub>. Maximum solubility performances were obtained via the highest achieved experimental pressure at 50 bars, reported in Table 2. For all cases, except for Be:La + CO<sub>2</sub> (Figure 2b), HBA experimental sorption performances was superior than that of HBD, which was also mentioned by D.O. Abranchesn et al. (that Be possess weak interaction with itself, but act as excellent HBA) [66]. ChCl+CO<sub>2</sub> showed the best performance with 4.96 mmol CO<sub>2</sub>/g, whereas Al + CO<sub>2</sub> showed the worst capture performance with 3.86 mmol CO<sub>2</sub>/g. In the case of Be:La + CO<sub>2</sub>, the NADES + CO<sub>2</sub> profile was observed to be lower than its constituents (Be and La), which can be explained due to the negative excess volume that was created via mixing the HBA and HBD [67]. Likewise, in the case of Al:Ma + CO<sub>2</sub>, the NADES profile was observed to be higher than its HBA and HBD, which is a sign of positive excess volume when Al and Ma was mixed to form NADES.

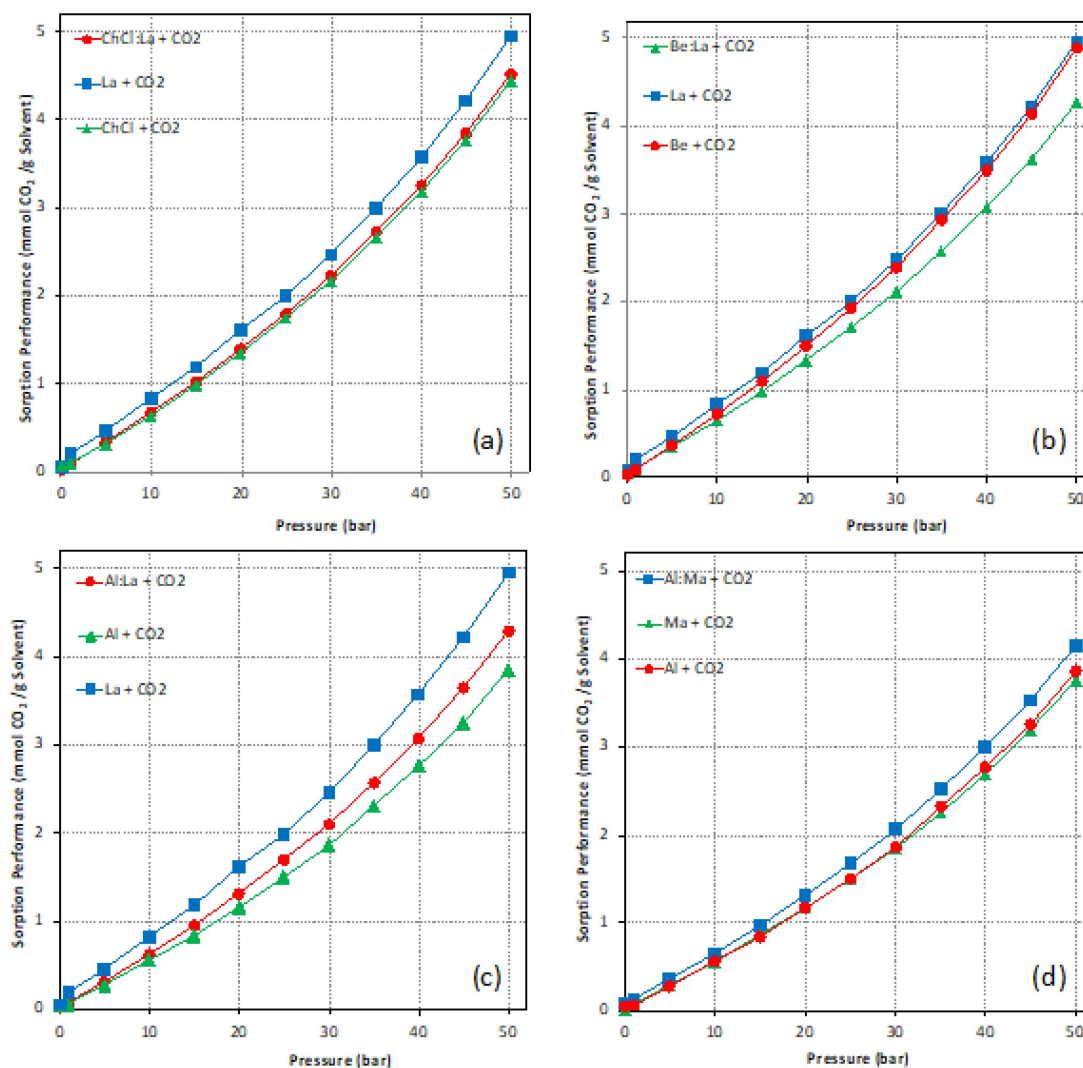


**Figure 2.** CO<sub>2</sub> capture performance of studied deep eutectic solvents (DES) systems and comparison to their constituents. (a) ChCl:La + CO<sub>2</sub>, (b) Be:La + CO<sub>2</sub>, (c) Al:La + CO<sub>2</sub>, (d) Al:Ma + CO<sub>2</sub>.

**Table 2.** Gas sorption data and binding energies ranking.

Structure	Sorption (mmol CO <sub>2</sub> /g)	Sorption Comparison	Binding Energy (eV)	Binding Comparison
ChCl + CO <sub>2</sub>	4.96		−0.137	
ChCl:La + CO <sub>2</sub>	4.52	HBA > NADES > HBD	1.433	HBA > HBD
La + CO <sub>2</sub>	4.46		−0.122	
Be + CO <sub>2</sub>	4.88		−0.112	
Be:La + CO <sub>2</sub>	4.26	HBA > HBD > NADES	1.292	HBD > HBA
La + CO <sub>2</sub>	4.46		−0.122	
Al + CO <sub>2</sub>	3.86		−0.119	
Al:La + CO <sub>2</sub>	4.30	HBD > NADES > HBA	0.828	HBA ~ HBD
La + CO <sub>2</sub>	4.46		−0.122	
Al + CO <sub>2</sub>	3.86		−0.119	
Al:Ma + CO <sub>2</sub>	4.14	NADES > HBA > HBD	N/A	HBA > HBD
Ma + CO <sub>2</sub>	3.76		−0.104	
ChCl + CO <sub>2</sub>	4.96		−0.137	
ChCl:Fr + CO <sub>2</sub>	4.24	HBA > NADES > HBD	2.199	HBA > HBD
Fr + CO <sub>2</sub>	3.58		−0.101	
ChCl + CO <sub>2</sub>	4.96		−0.137	
ChCl:Ma + CO <sub>2</sub>	4.22	HBA > NADES > HBD	1.514	HBA > HBD
Ma + CO <sub>2</sub>	3.76		−0.104	

As clearly reported in Table 1, the CO<sub>2</sub> capture performance of NADES is lower in comparison to sole HBA and HBD cases, for most of the studied cases. When the melting point of the studied HBA and HBD are considered, they are solid in room temperatures, and even at elevated process temperatures, at which typical pre- and post-combustion CO<sub>2</sub> capture operations take place. However, the NADES compounds exist in liquid phase at mentioned temperatures, thus, making their processability much easier than their constituents. One of the main objectives of considering solvents for CO<sub>2</sub> capture is to be able to utilize existing infrastructures that were built with the consideration of current-state-of-the-art capture agents (e.g., monoethanolamine-based solvents), with minimum retrofitting requirements on the equipment infrastructure.

DFT simulations were carried out for the same structures for which the experimental findings were shared above. The main purpose of the utilization DFT simulations was to obtain insights on electronic configuration of the studied compounds and infer on the behavior of the interaction sites between the HBA/HBD/NADES structures and the CO<sub>2</sub> molecule. Macroscopic properties can be estimated through calculation intensive molecular dynamic simulations. DFT simulations were carried out for each NADES, HBA, and HBD with CO<sub>2</sub> gas presented around them at various spatial positions. Three different spatial positions were considered for potentially high CO<sub>2</sub> interactions sites for NADES and two positions were considered for HBA/HBD compounds, respectively. Obviously, a restricted amount of CO<sub>2</sub> molecules around the NADES structure would not represent the overall bulk phase conditions and the entire solubility phenomena. It should be noted that DFT is considered a tool to assess the interaction nature as well as characteristics of the studied compounds in case they are exposed to CO<sub>2</sub>.

Once the DFT simulations were obtained and the interactions energies were corrected for the BSSE [59], the cases that gave the highest interaction energies were considered for further DFT analysis. In this work B3LYP with the 6-311++G\*\* theory level was selected, based on its accuracy and reasonable computational time [49,50]. The summary of interaction energies for the selected cases are provided in Table 3 in eV units. Binding energies for each HBA, HBD, and NADES with CO<sub>2</sub> are provided in Table 4, along with comparisons of binding energies with respect to each other within each NADES group.

**Table 3.** Summary of energies of optimized structures.

Group	Structure	Energy (eV)
NADES	Al:La	−18,157.79
	Be:La	−20,295.39
	ChCl:Fr	−40,166.78
	ChCl:La	−30,819.46
	ChCl:Ma	−35,950.19
Gas	CO <sub>2</sub>	−5,131.10
HBD	La	−9,348.54
	Fr	−18,695.51
	Ma	−14,479.15
HBA	Al	−8,807.68
	Be	−10,944.60
	ChCl	−21,468.77

**Table 4.** Optimized energies of HBA, HBD, and natural deep eutectic solvents (NADES) interacting with CO<sub>2</sub> at various spatial positions.

Group	Structure	Energy (eV)	Binding Energy (eV)	Average Binding Energy (eV)
NADES + CO <sub>2</sub>	Al:La + CO <sub>2</sub> _p1	−23,288.051	0.840	0.828
	Al:La + CO <sub>2</sub> _p2	−23,288.072	0.819	
	Al:La + CO <sub>2</sub> _p3	−23,288.065	0.826	
	Be:La + CO <sub>2</sub> _p1	−25,425.242	1.248	1.292
	Be:La + CO <sub>2</sub> _p2	−25,425.200	1.289	
	Be:La + CO <sub>2</sub> _p3	−25,425.150	1.339	
	ChCl:Fr + CO <sub>2</sub> _p1	−45,295.714	2.167	2.199
	ChCl:Fr + CO <sub>2</sub> _p2	−45,295.679	2.202	
	ChCl:Fr + CO <sub>2</sub> _p3	−45,295.654	2.227	
	ChCl:La + CO <sub>2</sub> _p1	−35,949.184	1.370	1.433
	ChCl:La + CO <sub>2</sub> _p2	−35,949.103	1.451	
	ChCl:La + CO <sub>2</sub> _p3	−35,949.075	1.478	
	ChCl:Ma + CO <sub>2</sub> _p1	−41,079.907	1.379	1.514
	ChCl:Ma + CO <sub>2</sub> _p2	−41,079.733	1.553	
	ChCl:Ma + CO <sub>2</sub> _p3	−41,079.676	1.610	
HBA + CO <sub>2</sub>	Al + CO <sub>2</sub> _p1	−13,938.915	−0.138	−0.119
	Al + CO <sub>2</sub> _p2	−13,938.876	−0.099	
	Be + CO <sub>2</sub> _p1	−16,075.871	−0.173	−0.112
	Be + CO <sub>2</sub> _p2	−16,075.749	−0.051	
	ChCl + CO <sub>2</sub> _P1	−26,600.028	−0.158	−0.137
	ChCl + CO <sub>2</sub> _P2	−26,599.997	−0.127	
ChCl + CO <sub>2</sub> _P3	−26,599.996	−0.126		

Table 4. Cont.

Group	Structure	Energy (eV)	Binding Energy (eV)	Average Binding Energy (eV)
HBD + CO <sub>2</sub>	Fr + CO <sub>2</sub> _p1	-23,826.696	-0.093	-0.101
	Fr + CO <sub>2</sub> _p2	-23,826.712	-0.108	
	La + CO <sub>2</sub> _p1	-14,479.781	-0.145	-0.122
	La + CO <sub>2</sub> _p2	-14,479.736	-0.099	
	Ma + CO <sub>2</sub> _p1	-19,610.352	-0.101	-0.104
	Ma + CO <sub>2</sub> _p2	-19,610.358	-0.106	

Once the binding energy results are deeply analyzed, HBA > HBD trend is observed for CO<sub>2</sub> interactions, which is similar to the experimental behavior CO<sub>2</sub> sorption performance in HBA/HBD. The only exception was observed in Be + CO<sub>2</sub> and La + CO<sub>2</sub> comparisons, for which the binding energy is higher for HBD + CO<sub>2</sub> than HBA + CO<sub>2</sub> case. There is no particular correlation between the maximum sorption amount and the binding energy for the NADES + CO<sub>2</sub> cases. On the other hand, the maximum sorption amounts and the binding energies for both HBD and HBA follows the same rank. In other words, it was observed that as the binding energy for CO<sub>2</sub> increases, the CO<sub>2</sub> sorption performance also increases for both HBD and HBA cases.

Furthermore, the interfacial properties of NADES/HBA/HBD and CO<sub>2</sub> can also be studied using molecular dynamics simulations. Garcia et al. showed how CO<sub>2</sub> establishes remarkable interactions with the bulk NADES structure through analyzing the evolution of the number of hydrogen bondings between the HBA and HBD [46]. Furthermore, strong affinity between DES and CO<sub>2</sub> molecules were quantified by the corresponding interaction energies. Results shared by Garcia et al. showed the large interaction energies for interaction of CO<sub>2</sub> molecules, with both the HBA and HBD, with slightly higher values between HBA and CO<sub>2</sub> in comparison to HBD–CO<sub>2</sub>. Relatively small differences between the HBA and CO<sub>2</sub> and HBD–CO<sub>2</sub> suggests a mutual effect on CO<sub>2</sub> solubility [46].

On the other hand, a study by Wang et al. showed the effect of the type and molar mixing ratio of HBA and HBD for ionic liquid-based DES through analyzing the radial distribution functions. It was reported that the cation of the HBA plays a superior role on the hydrogen bond development between the DES and CO<sub>2</sub>, yet again supporting the observed trend in this work [68].

Another molecular dynamics-based study that supports the CO<sub>2</sub> affinity is driven by HBA of the DES was reported elsewhere [69]. Besides analyzing the hydrogen bond evolution between the CO<sub>2</sub> molecule and HBA/HBD, they proved the superior effect of HBA on CO<sub>2</sub> affinity via displaying the higher degree of clustering of CO<sub>2</sub> molecules around the HBA through the spatial distribution function isosurfaces. All of these studies are in line with the arguments that are claimed in this work through DFT simulations on the superior binding effect of HBA on CO<sub>2</sub>.

The reduced density gradients (RDG) isosurfaces were used to visualize the interaction of CO<sub>2</sub> with HBA and HBD, Figure 3. Strong van der Waals type interactions are recorded for CO<sub>2</sub> binding at relevant interaction sites at HBA and HBD, which is a sign of reversible process for CO<sub>2</sub> sorption since H-bonding has not been observed. Especially at ChCl, both -H and -Cl<sup>-</sup> sites showed more intensified RDG volumes between the -O site of CO<sub>2</sub> (Figure 3c), which is also quantified with the highest binding energy with -0.137 eV (Table 2). Likewise, weakest interaction was observed with less intense isosurface between CO<sub>2</sub> and Ma (Figure 3e), and it is evident with the binding energy reported in Table 2 for Ma + CO<sub>2</sub>.

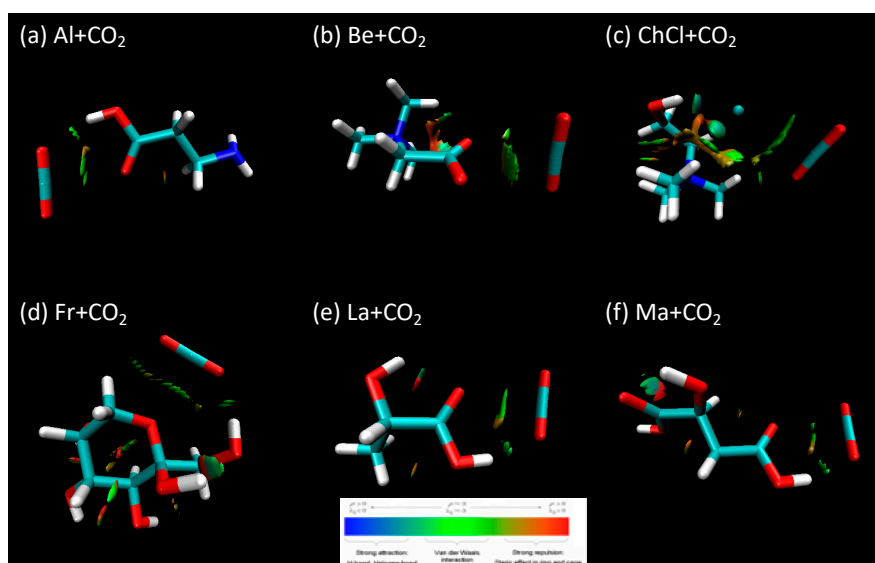


**Figure 3.** Reduced Density Gradient (RDG) isosurfaces for HBA + CO<sub>2</sub> and HBD + CO<sub>2</sub> cases. (a) Al + CO<sub>2</sub>, (b) Be + CO<sub>2</sub>, (c) ChCl + CO<sub>2</sub>, (d) Fr + CO<sub>2</sub>, (e) La + CO<sub>2</sub>, (f) Ma + CO<sub>2</sub>.

Quantum theory atom-in-a-molecule (QTAIM) analysis and RDG isosurfaces for NADES was presented for NADES + CO<sub>2</sub> cases in Figures 4 and 5, respectively. For most of the cases, CO<sub>2</sub> established critical binding with HBA of the NADES structure, except for the ChCl:Fr + CO<sub>2</sub> case. In Figure 4, it is evident that -O site of CO<sub>2</sub> is the most recurring interaction between the HBA -H site. The experimental values for the CO<sub>2</sub> solubility in NADES can be ranked as ChCl:La > Al:La ~ ChCl:Ma > Be:La > Al:La. Whereas the binding energies that are calculated via DFT simulations for CO<sub>2</sub> are ranked as ChCl:Fr > ChCl:La ~ ChCl:Ma > Be:La > Al:La. These two comparisons do not overlap with each other. A more logical comparison on overall solubility performance, with respect to binding energies, would be between the NADES constituent prior to the mixing, since they form excess volume pockets once they are mixed, which leads to excess CO<sub>2</sub> capture performance.

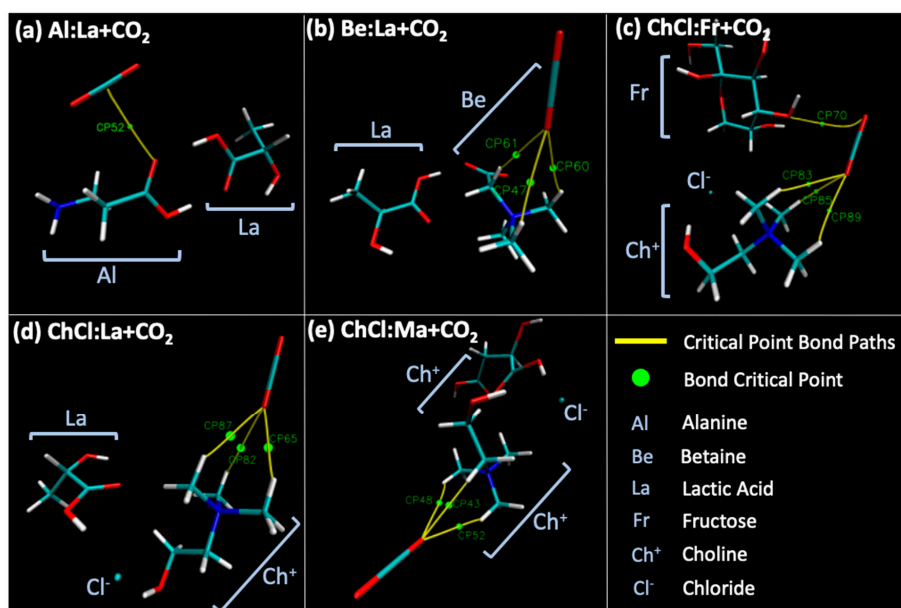


**Figure 4.** Density functional theory (DFT) figures for each structure final optimized geometry.

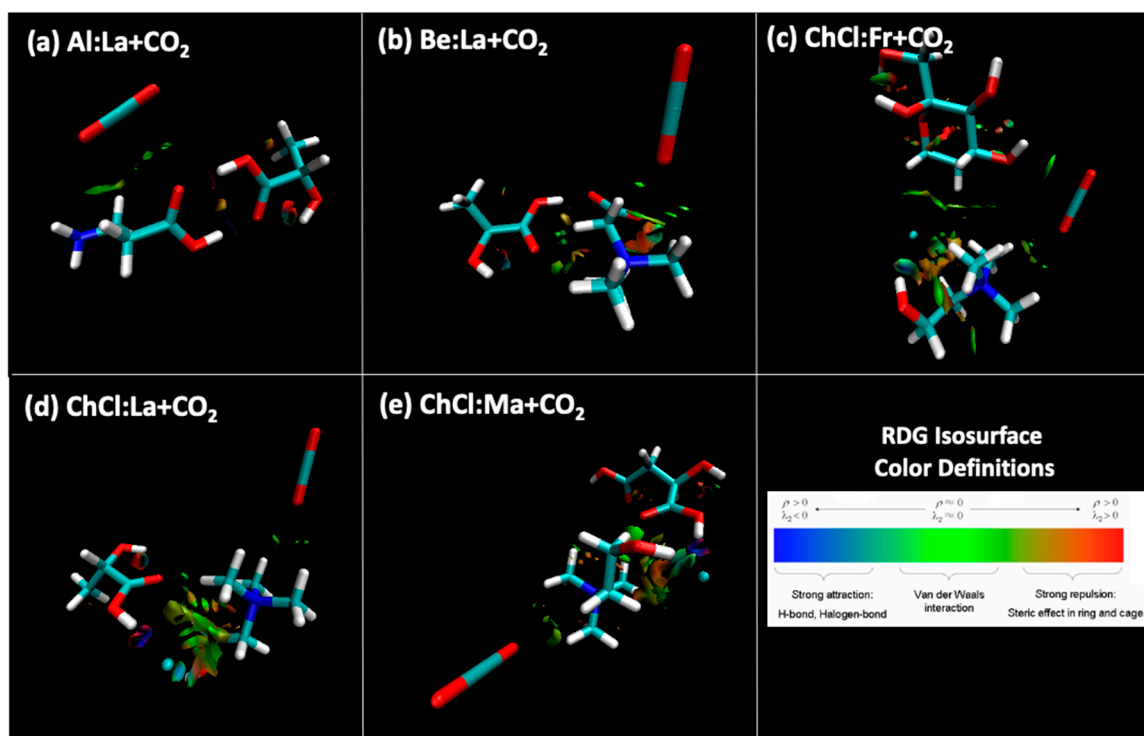


Figure 5. Reduced density gradient (RDG) isosurfaces for HBA + CO<sub>2</sub> and HBD + CO<sub>2</sub> cases.

#### 4. Conclusions

In this study, the mechanism of CO<sub>2</sub> sorption amino acid based NADES, the effect of the hydrogen bond acceptor and hydrogen bond donor on carbon dioxide absorption via natural deep eutectic solvent systems is presented for the first time. These results will assist the scientific community while designing NADES for gas sorption applications. Both experimental and DFT simulation for NADES, HBA, and HBD were studied for their CO<sub>2</sub> sorption performances. Strong van der Waals forces were observed as binding characteristics of CO<sub>2</sub> with all of the studied cases, which supports the physisorption behavior of the HBA + CO<sub>2</sub>, HBD + CO<sub>2</sub>, as well as NADES + CO<sub>2</sub> experimental behavior that did not yield any adsorption-desorption hysteresis. Furthermore, it has been observed that HBA plays a leading role in CO<sub>2</sub> solubility for NADES cases. Polarity unbalance of Be and ChCl based NADES cases causes strong negative deviations from ideality when mixed with their organic HBD. This effect was also observed on the CO<sub>2</sub> absorption plots (Figure 2), at which the NADES solubility performances were pushed further down, yielding lower performance in comparison to both HBA and HBD. Furthermore, considering Be and ChCl cases, both the experimental sorption and theoretical interaction energies are close to each other and higher than that of the Al cases. This could be explained, due to both HBA forming a positive charge shielded by alkyl groups, forming stronger intra H-bonding between the HBA and HBD, which also leads to larger interactions with surrounding CO<sub>2</sub> molecule. Furthermore, such strong H-bonding establishment in between the HBA and HBD, for all cases, but specific to Be and ChCl cases, negative deviations from ideality in mixture, can be correlated to higher CO<sub>2</sub> affinity establishment. Additionally, the strong H-bonding between HBA and HBD leads to very strong NADES structure and, thus, no disruption effect has been noticed when the NADES compounds were exposed to the CO<sub>2</sub> environment. Consequently, the characteristics of NADES has been preserved in these cases. For novel solvent design via DES or NADES, in order to confirm the leading effect of HBA for gas solubility, there is a need for a more systematic analysis, especially considering a wider range of HBA and HBD, as well as different gases.

**Supplementary Materials:** The following are available online at <http://www.mdpi.com/2227-9717/8/12/1533/s1>, Figure S1: title. CO<sub>2</sub> capture performance for hydrogen bond acceptors and hydrogen bond donors prior to mixing to form deep eutectic solvent at 298.15 K isotherm with (mol CO<sub>2</sub>/mol solvent units).

**Author Contributions:** Conceptualization, T.A., S.A. and M.A.; methodology, S.A. and M.A.; software, S.A. and M.A.; validation, T.A., S.A. and M.A.; formal analysis, T.A., A.A., S.A. and M.A.; investigation, S.A. and M.A.; resources, A.A., S.A. and M.A.; data curation, M.A.; writing—original draft preparation, T.A., S.A. and M.A.; writing—review and editing, T.A., A.A., S.A. and M.A.; visualization, M.A.; supervision, A.A., S.A. and M.A.; project administration, M.A. All authors have read and agreed to the published version of the manuscript.

**Funding:** This research received no external funding.

**Acknowledgments:** The authors acknowledge SCAYLE (Supercomputación Castilla y León, Burgos, Spain) for providing supercomputing facilities. The statements made herein are solely the responsibility of the authors.

**Conflicts of Interest:** The authors declare no conflict of interest.

## References

- Macário, I.P.E.; Oliveira, H.; Menezes, A.C.; Ventura, S.P.M.; Pereira, J.L.; Gonçalves, A.M.M.; Coutinho, J.A.P.; Gonçalves, F.J.M. Cytotoxicity profiling of deep eutectic solvents to human skin cells. *Sci. Rep.* **2019**, *9*, 3932. [[CrossRef](#)]
- Halder, A.K.; Cordeiro, M.N.D.S. Probing the Environmental Toxicity of Deep Eutectic Solvents and Their Components: An In Silico Modeling Approach. *ACS Sustain. Chem. Eng.* **2019**, *7*, 10649–10660. [[CrossRef](#)]
- Valencia-Marquez, D.; Flores-Tlacuahuac, A.; Vasquez-Medrano, R. An optimization approach for CO<sub>2</sub> capture using ionic liquids. *J. Clean. Prod.* **2017**, *168*, 1652–1667. [[CrossRef](#)]
- Bi, Y.; Hu, Z.; Lin, X.; Ahmad, N.; Xu, J.; Xu, X. Efficient CO<sub>2</sub> capture by a novel deep eutectic solvent through facile, one-pot synthesis with low energy consumption and feasible regeneration. *Sci. Total Environ.* **2020**, *705*, 135798. [[CrossRef](#)]
- Leron, R.B.; Li, M.-H. Solubility of carbon dioxide in a choline chloride–ethylene glycol based deep eutectic solvent. *Thermochim. Acta* **2013**, *551*, 14–19. [[CrossRef](#)]
- Sreedhar, I.; Nahar, T.; Venugopal, A.; Srinivas, B. Carbon capture by absorption—Path covered and ahead. *Renew. Sustain. Energy Rev.* **2017**, *76*, 1080–1107. [[CrossRef](#)]
- Mirza, N.; Mumford, K.; Wu, Y.; Mazhar, S.; Kentish, S.; Stevens, G. Improved Eutectic Based Solvents for Capturing Carbon Dioxide (CO<sub>2</sub>). *Energy Procedia* **2017**, *114*, 827–833. [[CrossRef](#)]
- Hjelmaas, S.; Storheim, E.; Flø, N.E.; Thorjussen, E.S.; Morken, A.K.; Faramarzi, L.; de Cazenove, T.; Hamborg, E.S. Results from MEA Amine Plant Corrosion Processes at the CO<sub>2</sub> Technology Centre Mongstad. *Energy Procedia* **2017**, *114*, 1166–1178. [[CrossRef](#)]
- Husebye, J.; Brunsvold, A.L.; Roussanaly, S.; Zhang, X. Techno Economic Evaluation of Amine based CO<sub>2</sub> Capture: Impact of CO<sub>2</sub> Concentration and Steam Supply. *Energy Procedia* **2012**, *23*, 381–390. [[CrossRef](#)]
- Davis, J.; Rochelle, G. Thermal degradation of monoethanolamine at stripper conditions. *Energy Procedia* **2009**, *1*, 327–333. [[CrossRef](#)]
- Luis, P. Use of monoethanolamine (MEA) for CO<sub>2</sub> capture in a global scenario: Consequences and alternatives. *Desalination* **2016**, *380*, 93–99. [[CrossRef](#)]
- Abotaleb, A.; El-Naas, M.; Amhamed, A. Enhancing gas loading and reducing energy consumption in acid gasremoval systems: A simulation study based on real NGL plant data. *J. Nat. Gas Sci. Eng.* **2018**, *55*, 565–574. [[CrossRef](#)]
- Rozyyev, V.; Thirion, D.; Ullah, R.; Lee, J.; Jung, M.; Oh, H.; Atilhan, M.; Yavuz, C.T. High-capacity methane storage in flexible alkane-linked porous aromatic network polymers. *Nat. Energy* **2019**, *4*, 604–611. [[CrossRef](#)]
- Furukawa, H.; Cordova, K.E.; O’Keeffe, M.; Yaghi, O.M. The Chemistry and Applications of Metal-Organic Frameworks. *Science* **2013**, *341*, 1230444. [[CrossRef](#)]
- Megías-Sayago, C.; Bingre, R.; Huang, L.; Lutzweiler, G.; Wang, Q.; Louis, B. CO<sub>2</sub> Adsorption Capacities in Zeolites and Layered Double Hydroxide Materials. *Front. Chem.* **2019**, *7*, 551. [[CrossRef](#)]
- Titinchi, S.J.J. Chemically Modified Solid Adsorbents for CO<sub>2</sub> Capture. *Energy Procedia* **2014**, *8*, 8153–8160. [[CrossRef](#)]
- Jiang, L.; Gonzalez-Diaz, A.; Ling-Chin, J.; Roskilly, A.P.; Smallbone, A.J. Post-combustion CO<sub>2</sub> capture from a natural gas combined cycle power plant using activated carbon adsorption. *Appl. Energy* **2019**, *245*, 1–15. [[CrossRef](#)]

18. Closmann, F.; Nguyen, T.; Rochelle, G.T. MDEA/Piperazine as a solvent for CO<sub>2</sub> capture. *Energy Procedia* **2009**, *1*, 1351–1357. [[CrossRef](#)]
19. Liu, J.; Li, X.; Zhang, Z.; Li, L.; Bi, Y.; Zhang, L. Promotion of CO<sub>2</sub> capture performance using piperazine (PZ) and diethylenetriamine (DETA) bi-solvent blends. *Greenh. Gases Sci. Technol.* **2019**, *9*, 349–359. [[CrossRef](#)]
20. Aghaie, M.; Rezaei, N.; Zendehboudi, S. A systematic review on CO<sub>2</sub> capture with ionic liquids: Current status and future prospects. *Renew. Sustain. Energy Rev.* **2018**, *96*, 502–525. [[CrossRef](#)]
21. Ramdin, M.; de Loos, T.W.; Vlugt, T.J.H. State-of-the-Art of CO<sub>2</sub> Capture with Ionic Liquids. *Ind. Eng. Chem. Res.* **2012**, *51*, 8149–8177. [[CrossRef](#)]
22. Chong, F.K.; Chemmangattavalappil, N.; Foo, D.C.Y.; Atilhan, M.; Eljack, F.T. Ionic Liquid Mixture Design for Carbon Capture using Property Clustering Technique. *Chem. Eng. Trans.* **2015**, *45*, 1567–1572. [[CrossRef](#)]
23. Shiflett, M.B.; Drew, D.W.; Cantini, R.A.; Yokozeki, A. Carbon Dioxide Capture Using Ionic Liquid 1-Butyl-3-methylimidazolium Acetate. *Energy Fuels* **2010**, *24*, 5781–5789. [[CrossRef](#)]
24. García, G.; Atilhan, M.; Aparicio, S. Simultaneous CO<sub>2</sub> and SO<sub>2</sub> capture by using ionic liquids: A theoretical approach. *Phys. Chem. Chem. Phys.* **2017**, *19*, 5411–5422. [[CrossRef](#)] [[PubMed](#)]
25. Rafat, A.; Atilhan, M.; Kahraman, R. Corrosion Behavior of Carbon Steel in CO<sub>2</sub> Saturated Amine and Imidazolium-, Ammonium-, and Phosphonium-Based Ionic Liquid Solutions. *Ind. Eng. Chem. Res.* **2016**, *55*, 446–454. [[CrossRef](#)]
26. Bhawna; Pandey, A.; Dhingra, D.; Pandey, S. Can common liquid polymers and surfactants capture CO<sub>2</sub>? *J. Mol. Liq.* **2019**, *277*, 594–605. [[CrossRef](#)]
27. Zulfiqar, S.; Ilyas Sarwar, M.; Mecerreyes, D. Polymeric ionic liquids for CO<sub>2</sub> capture and separation: Potential, progress and challenges. *Polym. Chem.* **2015**, *6*, 6435–6451. [[CrossRef](#)]
28. Kupgan, G.; Abbott, L.J.; Hart, K.E.; Colina, C.M. Modeling Amorphous Microporous Polymers for CO<sub>2</sub> Capture and Separations. *Chem. Rev.* **2018**, *118*, 5488–5538. [[CrossRef](#)]
29. Zhang, J.; Chai, S.-H.; Qiao, Z.-A.; Mahurin, S.M.; Chen, J.; Fang, Y.; Wan, S.; Nelson, K.; Zhang, P.; Dai, S. Porous Liquids: A Promising Class of Media for Gas Separation. *Angew. Chem.* **2015**, *127*, 946–950. [[CrossRef](#)]
30. Zhang, N.; Huang, Z.; Zhang, H.; Ma, J.; Jiang, B.; Zhang, L. Highly Efficient and Reversible CO<sub>2</sub> Capture by Task-Specific Deep Eutectic Solvents. *Ind. Eng. Chem. Res.* **2019**, *58*, 13321–13329. [[CrossRef](#)]
31. Trivedi, T.J.; Lee, J.H.; Lee, H.J.; Jeong, Y.K.; Choi, J.W. Deep eutectic solvents as attractive media for CO<sub>2</sub> capture. *Green Chem.* **2016**, *18*, 2834–2842. [[CrossRef](#)]
32. García, G.; Aparicio, S.; Ullah, R.; Atilhan, M. Deep Eutectic Solvents: Physicochemical Properties and Gas Separation Applications. *Energy Fuels* **2015**, *29*, 2616–2644. [[CrossRef](#)]
33. Ren, H.; Lian, S.; Wang, X.; Zhang, Y.; Duan, E. Exploiting the hydrophilic role of natural deep eutectic solvents for greening CO<sub>2</sub> capture. *J. Clean. Prod.* **2018**, *193*, 802–810. [[CrossRef](#)]
34. Mulia, K.; Putri, S.; Krisanti, E.; Nasruddin. Natural deep eutectic solvents (NADES) as green solvents for carbon dioxide capture. *AIP Conf. Proc.* **2017**, *1823*, 020022. [[CrossRef](#)]
35. Amhamed, A.; Atilhan, M.; Berdiyrov, G. Permeabilities of CO<sub>2</sub>, H<sub>2</sub>S and CH<sub>4</sub> through Choline-Based Ionic Liquids: Atomistic-Scale Simulations. *Molecules* **2019**, *24*, 2014. [[CrossRef](#)]
36. Ma, C.; Sarmad, S.; Mikkola, J.-P.; Ji, X. Development of Low-Cost Deep Eutectic Solvents for CO<sub>2</sub> Capture. *Energy Procedia* **2017**, *142*, 3320–3325. [[CrossRef](#)]
37. Cruz, H.; Jordão, N.; Branco, L.C. Deep eutectic solvents (DESs) as low-cost and green electrolytes for electrochromic devices. *Green Chem.* **2017**, *19*, 1653–1658. [[CrossRef](#)]
38. Ullah, R.; Atilhan, M.; Anaya, B.; Khraisheh, M.; García, G.; ElKhattat, A.; Tariq, M.; Aparicio, S. A detailed study of cholinium chloride and levulinic acid deep eutectic solvent system for CO<sub>2</sub> capture via experimental and molecular simulation approaches. *Phys. Chem. Chem. Phys.* **2015**, *17*, 20941–20960. [[CrossRef](#)]
39. Liu, Y.; Yu, H.; Sun, Y.; Zeng, S.; Zhang, X.; Nie, Y.; Zhang, S.; Ji, X. Screening Deep Eutectic Solvents for CO<sub>2</sub> Capture with COSMO-RS. *Front. Chem.* **2020**, *8*, 82. [[CrossRef](#)]
40. Paiva, A.; Craveiro, R.; Aroso, I.; Martins, M.; Reis, R.L.; Duarte, A.R.C. Natural Deep Eutectic Solvents–Solvents for the 21st Century. *ACS Sustain. Chem. Eng.* **2014**, *2*, 1063–1071. [[CrossRef](#)]
41. Isaifan, R.J.; Amhamed, A. Review on Carbon Dioxide Absorption by Choline Chloride/Urea Deep Eutectic Solvents. *Adv. Chem.* **2018**, *2018*, 2675659. [[CrossRef](#)]
42. Gu, Y.; Hou, Y.; Ren, S.; Sun, Y.; Wu, W. Hydrophobic Functional Deep Eutectic Solvents Used for Efficient and Reversible Capture of CO<sub>2</sub>. *ACS Omega* **2020**, *5*, 6809–6816. [[CrossRef](#)] [[PubMed](#)]

43. Abbott, A.P.; Boothby, D.; Capper, G.; Davies, D.L.; Rasheed, R.K. Deep Eutectic Solvents Formed between Choline Chloride and Carboxylic Acids: Versatile Alternatives to Ionic Liquids. *J. Am. Chem. Soc.* **2004**, *126*, 9142–9147. [[CrossRef](#)] [[PubMed](#)]
44. Sze, L.L.; Pandey, S.; Ravula, S.; Pandey, S.; Zhao, H.; Baker, G.A.; Baker, S.N. Ternary Deep Eutectic Solvents Tasked for Carbon Dioxide Capture. *ACS Sustain. Chem. Eng.* **2014**, *2*, 2117–2123. [[CrossRef](#)]
45. Sarmad, S.; Mikkola, J.-P.; Ji, X. Carbon Dioxide Capture with Ionic Liquids and Deep Eutectic Solvents: A New Generation of Sorbents. *ChemSusChem* **2017**, *10*, 324–352. [[CrossRef](#)]
46. García, G.; Atilhan, M.; Aparicio, S. Interfacial Properties of Deep Eutectic Solvents Regarding to CO<sub>2</sub> Capture. *J. Phys. Chem. C* **2015**, *119*, 21413–21425. [[CrossRef](#)]
47. Zubeir, L.F.; van Osch, D.J.G.P.; Rocha, M.A.A.; Banat, F.; Kroon, M.C. Carbon Dioxide Solubilities in Decanoic Acid-Based Hydrophobic Deep Eutectic Solvents. *J. Chem. Eng. Data* **2018**, *63*, 913–919. [[CrossRef](#)]
48. Haider, M.B.; Jha, D.; Marriyappan Sivagnanam, B.; Kumar, R. Thermodynamic and Kinetic Studies of CO<sub>2</sub> Capture by Glycol and Amine-Based Deep Eutectic Solvents. *J. Chem. Eng. Data* **2018**, *63*, 2671–2680. [[CrossRef](#)]
49. Altamash, T.; Amhamed, A.I.; Aparicio, S.; Atilhan, M. Combined Experimental and Theoretical Study on High Pressure Methane Solubility in Natural Deep Eutectic Solvents. *Ind. Eng. Chem. Res.* **2019**, *58*, 8097–8111. [[CrossRef](#)]
50. Altamash, T.; Nasser, M.S.; Elhamarnah, Y.; Magzoub, M.; Ullah, R.; Qiblawey, H.; Aparicio, S.; Atilhan, M. Gas solubility and rheological behavior study of betaine and alanine based natural deep eutectic solvents (NADES). *J. Mol. Liq.* **2018**, *256*, 286–295. [[CrossRef](#)]
51. Altamash, T.; Nasser, M.S.; Elhamarnah, Y.; Magzoub, M.; Ullah, R.; Anaya, B.; Aparicio, S.; Atilhan, M. Gas Solubility and Rheological Behavior of Natural Deep Eutectic Solvents (NADES) via Combined Experimental and Molecular Simulation Techniques. *ChemistrySelect* **2017**, *2*, 7278–7295. [[CrossRef](#)]
52. Ebner, A.D.; Gray, M.L.; Chisholm, N.G.; Black, Q.T.; Mumford, D.D.; Nicholson, M.A.; Ritter, J.A. Suitability of a Solid Amine Sorbent for CO<sub>2</sub> Capture by Pressure Swing Adsorption. *Ind. Eng. Chem. Res.* **2011**, *50*, 5634–5641. [[CrossRef](#)]
53. Karadas, F.; Yavuz, C.T.; Zulfiqar, S.; Aparicio, S.; Stucky, G.D.; Atilhan, M. CO<sub>2</sub> Adsorption Studies on Hydroxy Metal Carbonates M(CO<sub>3</sub>)<sub>x</sub>(OH)<sub>y</sub> (M = Zn, Zn–Mg, Mg, Mg–Cu, Cu, Ni, and Pb) at High Pressures up to 175 bar. *Langmuir* **2011**, *27*, 10642–10647. [[CrossRef](#)] [[PubMed](#)]
54. Adams, S.; De Castro, P.; Echenique, P.; Estrada, J.; Hanwell, M.D.; Murray-Rust, P.; Sherwood, P.; Thomas, J.; Townsend, J. The Quixote project: Collaborative and Open Quantum Chemistry data management in the Internet age. *J. Cheminform.* **2011**, *3*, 38. [[CrossRef](#)] [[PubMed](#)]
55. Neese, F. The ORCA program system. *WIREs Comput. Mol. Sci.* **2012**, *2*, 73–78. [[CrossRef](#)]
56. Lee, C.; Yang, W.; Parr, R.G. Development of the Colle-Salvetti correlation-energy formula into a functional of the electron density. *Phys. Rev. B* **1988**, *37*, 785–789. [[CrossRef](#)] [[PubMed](#)]
57. Becke, A.D. Density-functional exchange-energy approximation with correct asymptotic behavior. *Phys. Rev. A* **1988**, *38*, 3098–3100. [[CrossRef](#)]
58. Grimme, S.; Antony, J.; Ehrlich, S.; Krieg, H. A consistent and accurate ab initio parametrization of density functional dispersion correction (DFT-D) for the 94 elements H–Pu. *J. Chem. Phys.* **2010**, *132*, 154104. [[CrossRef](#)]
59. Simon, S.; Duran, M.; Dannenberg, J.J. How does basis set superposition error change the potential surfaces for hydrogen-bonded dimers? *J. Chem. Phys.* **1996**, *105*, 11024–11031. [[CrossRef](#)]
60. Bader, R.F.W. *Atoms in Molecules: A Quantum Theory*; Clarendon Press: Oxford, UK, 1994.
61. Lu, T.; Chen, F. Multiwfn: A multifunctional wavefunction analyzer. *J. Comput. Chem.* **2012**, *33*, 580–592. [[CrossRef](#)]
62. Aparicio, S.; Yavuz, C.T.; Atilhan, M. Molecular Insights into Benzimidazole-Linked Polymer Interactions with Carbon Dioxide and Nitrogen. *ChemistrySelect* **2018**, *3*, 3691–3701. [[CrossRef](#)]
63. Xiao, J.; Zhao, Y.-P.; Fan, X.; Cao, J.-P.; Kang, G.-J.; Zhao, W.; Wei, X.-Y. Hydrogen bonding interactions between the organic oxygen/nitrogen monomers of lignite and water molecules: A DFT and AIM study. *Fuel Process. Technol.* **2017**, *168*, 58–64. [[CrossRef](#)]
64. Anbu, V.; Vijayalakshmi, K.A.; Karunathan, R.; Stephen, A.D.; Nidhin, P.V. Explosives properties of high energetic trinitrophenyl nitramide molecules: A DFT and AIM analysis. *Arab. J. Chem.* **2019**, *12*, 621–632. [[CrossRef](#)]

65. Johnson, E.R.; Keinan, S.; Mori-Sánchez, P.; Contreras-García, J.; Cohen, A.J.; Yang, W. Revealing Noncovalent Interactions. *J. Am. Chem. Soc.* **2010**, *132*, 6498–6506. [[CrossRef](#)] [[PubMed](#)]
66. Abranches, D.O.; Silva, L.P.; Martins, M.A.R.; Pinho, S.P.; Coutinho, J.A.P. Understanding the Formation of Deep Eutectic Solvents: Betaine as a Universal Hydrogen Bond Acceptor. *ChemSusChem* **2020**, *13*, 4916–4921. [[CrossRef](#)] [[PubMed](#)]
67. Crespo, E.A.; Costa, J.M.L.; Palma, A.M.; Soares, B.; Martín, M.C.; Segovia, J.J.; Carvalho, P.J.; Coutinho, J.A.P. Thermodynamic characterization of deep eutectic solvents at high pressures. *Fluid Phase Equilibria* **2019**, *500*, 112249. [[CrossRef](#)]
68. Wang, J.; Cheng, H.; Song, Z.; Chen, L.; Deng, L.; Qi, Z. Carbon Dioxide Solubility in Phosphonium-Based Deep Eutectic Solvents: An Experimental and Molecular Dynamics Study. *Ind. Eng. Chem. Res.* **2019**, *58*, 17514–17523. [[CrossRef](#)]
69. Altamash, T.; Atilhan, M.; Aliyan, A.; Ullah, R.; Garcia, G.; Aparicio, M. Insights into choline chloride-phenylacetic acid deep eutectic solvent for CO<sub>2</sub> absorption. *RSC Adv.* **2016**, *6*, 109201–109210. [[CrossRef](#)]

**Publisher's Note:** MDPI stays neutral with regard to jurisdictional claims in published maps and institutional affiliations.



© 2020 by the authors. Licensee MDPI, Basel, Switzerland. This article is an open access article distributed under the terms and conditions of the Creative Commons Attribution (CC BY) license (<http://creativecommons.org/licenses/by/4.0/>).